iC. 3

Applied Nuclear Data
Research and Development
Quarterly Progress Report

January 1 through March 31, 1974

Edited by

G. M. Hale
D. R. Harris
R. E. MacFarlane

los alamos
scientific laboratory
of the University of California
LOS ALAMOS, NEW MEXICO 87544

This report presents the status of the Applied Nuclear Data Research and Development Program. Other reports in this series, all unclassified, are:

LA-5546-PR

LA-5570-PR

In the interest of prompt distribution, this progress report was not edited by the Technical Information staff.

CONTENTS

Items I, II, III, V, VI, VII, X, and XIV include work for DRRD.
Items I, II, IV, VI, VIII, X, XI, XII, XIII, XIV, and XV include
work for DMA. Items XIII and XIV include work for DNA. Items I
and IX include work for DCTR. Items I, VI, VII, and XVIII in-
clude work for DRSR. Items XV and XVI include work for NASA.
Items VIII and XVII include work for NCI, University of Texas M.
D. Anderson Hospital and Tumor Institute, and Texas A & M Univer-
sity, and includes work carried out under the auspices of AWU.

APPLIED NUCLEAR DATA RESEARCH AND DEVELOPMENT

Edited by

G. M. Hale, D. R. Harris, and R. E. MacFarlane

ABSTRACT

This report presents progress in provision of nuclear data for nuclear design applications. The work described here is carried out through the LASL Applied Nuclear Data Group and covers the period January 1 through March 31, 1974. The topical content of this report is summarized in the Contents.

I. NUCLEAR CROSS-SECTION PROCESSING (P. D. Soran, R. E. MacFarlane, R. J. LaBauve, D. R. Harris, T. R. England, and D. W. Muir)

Group T-2 is supporting and developing a variety of computer codes for processing evaluated nuclear data into forms that can be used for design purposes. These include an advanced processor for groupwise neutron cross-sections (MINX),[1] a code which generates data for the LASL continuous energy Monte-Carlo codes (ETOPL), a gamma-ray production code (LAPHANO), and a photon interaction code (GAMLEG). In addition, there are a number of auxiliary processors for file management, plotting, data checking, and format conversion. Projects carried out this quarter related to these existing processors are described below under the following headings: Cross-Section Production, MINX Validation, Preliminary MINX Processed Data Library, MINX Code Development, and Other Code Development.

In order to provide advanced processing capabilities, allow for changed data formats (for example, ENDF/B-IV), and assure compatability between cross-sections, a new generation of processing modules is being developed. The four functions represented by the current codes will be unified into a single code system. Provision will also be made for processing functions not currently available at LASL such as thermal cross sections and delayed neutron production. The advanced code development is discussed under the heading MINX-II Code Development.

A. Cross-Section Production

During the quarter, multigroup cross sections for nitrogen (ENDF/B-IV MAT 4133) and oxygen (ENDF/B-IV MAT 4134) were provided for the LASL theoretical design division. The nitrogen were applied by H. A. Sandmeier (TD-6) to an air transport problem, and excellent agreement was noted by comparing with the results of continuous energy Monte Carlo techniques.[2] Also using MINX, multigroup cross sections for vanadium (ENDF/B-IV MAT 1196) and beryllium (ENDF/B-III MAT 1154) were prepared for fusion reactor studies in the LASL theoretical division.

B. MINX Validation

An extensive validation program has been laid out for the MINX processor. The first step is to process the "isotopes of tedium." These artificial isotopes are a CSEWG standard[3,4] for comparing processing codes. Each "isotope" is designed to test a particular format or method of calculation. For the tests on MINX, it was necessary to modify the official tedium deck by adding total and elastic cross sections and angular-distribution files. The 11 isotopes processed this quarter revealed minor errors in the linearization routine and in the integration procedure for the transfer matrices. After correcting these bugs, the cross sections produced by MINX were in excellent agreement with the results for other processing codes and with analytic results where available. Figure 1 shows the point-wise cross sections for tedium-16. This "isotope"
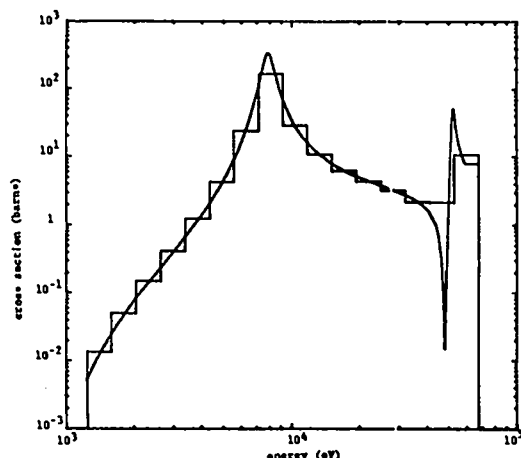
Fig. 1. Pointwise and groupwise (GAM-I struc-
ture) elastic scattering cross sections
for tedium-16, two wide s-wave reso-
nances with interference.

is based on the interfering resonances from iron.
The validation program will continue next quarter
with tests on real nuclides. The results will be
tested against other processing codes, the original
evaluations, hand calculations, and analytic re-
sults where possible.

C. Preliminary MINX Processed Data Library

Specifications have been established for pro-
cessing preliminary ENDF/B-IV data for Phase II data
testing in collaboration with G. Paik (Westinghouse
ARD) and B. Hutchins (GE-BRDO). The preliminary
library will include 22 nuclides of interest in the
fast breeder reactor program. The cross sections
will be in a 50 group structure at 4 temperatures
and 6 σ_0 values.

D. MINX Code Development

A major modification of the integration pro-
cedure for group averaging was made this quarter.
In earlier versions of MINX, a general adaptive in-
tegration procedure was employed which started at
the group boundaries and subdivided the group until
convergence was indicated. Subsequently it was dis-
covered that the adaptive procedure could break down
when there was a great deal of structure in the
cross section. It was decided to use an integration
procedure which included the union of all points ap-
pearing in the functions of the integrand, including
the weight function, the total cross-section and the
cross section being averaged. Because of the way
the pointwise cross sections are constructed in

MINX, this grid is guaranteed to reflect all the
structure in the integrand. Therefore, it is no
longer possible to miss a sharp peak. Various al-
ternatives were investigated for integrating the
panels defined by the unionized grid, including trap-
ezoidal, Simpson, analytic, and adaptive quadrature.
The last named method uses at least five integration
points per panel and was selected for all the group
averaging and transfer matrix calculations in MINX.

The second major modification to MINX was the
restructuring of the CCCC[5] output files. The ENDF/B
data is given from low to high energy and MINX pro-
cesses the data in this order (for simplified data
handling as well as paging capability). However,
the CCCC output files are structured from high to
low energy, and the transfer matrices are stored ac-
cording to sink group instead of source group. For
MINX to output cross sections in this fashion, major
data handling problems had to be overcome. Further-
more, handling of the CSEWG[6] 240 group library re-
quired the capability to read/write different size
records to minimize core requirements. These prob-
lems were solved by resorting to Large Core Memory
(LCM). The data handling restructuring also was
manifested in the BINX, LINX, and TINX codes and
modifications have begun on these auxiliary codes.

The unresolved resonance cross-section module
for MINX was completed and tested this quarter. It
uses the methods of the ETOX[7] code modified to fit
into the MINX structure. The cross sections are
computed at the limits of the unresolved energy
range and at any points in the file used to express
the energy dependence of the resonance parameters.
The code then goes through a linearization process
starting from this grid and adds any points needed
such that the unresolved resonance cross-section
can be represented by linear-linear interpolation
to a specified tolerance. These pointwise cross
sections agree with the cross sections generated by
the RESEND code at infinite dilution, and the group-
wise cross sections agree with those computed by
other processing codes for tedium-7 (see discussion
of tedium above).

E. Other Code Development

The MC[2] code system, which includes the codes
needed to prepare a data tape for MC[2] from an orig-
inal ENDF/B tape in addition to the MC[2] code proper,
was activated in linked fashion on the CDC-7600.

At the direction of the DRRD, this system was sent to the Swiss National Reactor Research Center, EIR (Eidg. Institute für Reaktorforschung) at Würenlingen, Switzerland.

F. MINX-II Code Development

The structure of MINX-II has been modified this quarter to use a new unified I/O system, to provide for an intermediate library of processed data in an ENDF/B-like format, and to allow for increased capabilities. All the modules of MINX-II communicate with each other through "tape" files of ENDF/B-type records. The records may be the standard BCD format or, for increased efficiency, they may have a new blocked binary structure which provides automatic paging and buffering. The unified I/O system takes care of all this overhead. It also provides for efficient buffered scratch storage in a machine-independent way.

Because of the wide range of users interested in the output of MINX, the Version II structure has been designed to provide a wide variety of output formats and collapse options. In order to make sure that all reactions on the ENDF/B tape are available, they are stored in an ENDF/B-like format under their original MT numbers on an intermediate library called GENDF (Groupwise ENDF). This file can then be processed by a collapse module and then passed through an output module to get the desired output format (CCCC, DTF, etc.).

The MINX-II structure is extremely modular. This allows new capabilities to be added to the program with a minimum effect on existing routines. The first stage of the new code will include the following capabilities: pointwise and groupwise neutron-induced self-shielded cross sections (including gamma production), pointwise and groupwise gamma-induced reaction cross sections (including photoneutron production), transfer matrices for all neutron and gamma reactions (n-n, n-γ, γ-γ, and γ-n), improved unresolved-resonance treatment with overlap effects, collapse to different group structure or P_N flux weighting with zero dimensional mixture capability, and output formats for CCC, DTF (separate or coupled sets), and the LASL continuous energy Monte Carlo codes. Subsequent phases may add thermal cross sections, probability tables for Monte Carlo codes, and delayed neutron production.

II. ADAPTIVE TRAPEZOIDAL AND Ax^B INTEGRATIONS (D. R. Harris and G. M. Hale)

Integrals of products of cross sections times fluxes and other weighting functions display considerable structure on scales of widely varying magnitudes. For example, a numerical integration over resonance cross sections may encounter wide resonances, very narrow resonances, and interference structures among them. Adaptive numerical integration algorithms are particularly appropriate for this application. Two adaptive integration algorithms, INTEG1 and INTEG2 have been developed for the STEEP and CINX codes containing a new feature—the forced inclusion of a data mesh in the integration mesh.

These algorithms first advance an interval of width DELT along the axis of integration, x, and compute the area of the panel, assuming that the integrand y(x) varies linearly (INTEG1) or as Ax^B (INTEG2) between x and x+DELT. Then the panel is divided in two and the integrals are computed between x and x+DELT/2 and between x+DELT/2 and x+DELT utilizing analogous assumptions. If the sum of the finer integrals is within a fraction EP of the larger integral, the algorithm steps ahead; if not, DELT is halved and the process is repeated.

This well-known technique can err when the integrand has excessive structure, e.g., a fine resonance can be skipped entirely. Hence, the technique has been modified so that the adaptive integration mesh is forced to include a data mesh, e.g., resonance energies, established outside the subroutines and brought in through a labeled COMMON. Figure 2 shows an error-computation time figure for two values of EP, for many values of DELT, and for an integration extending over (1,10) and including five resonances with widths between 1 and .001. All cases are at least an order of magnitude faster than non-adaptive integration;and, because the integration mesh was forced to include the five resonance energies, no resonance could be skipped.

III. TESTING OF NUCLEAR DATA OF IMPORTANCE IN SHIELDING APPLICATIONS AGAINST INTEGRAL EXPERIMENT (D. W. Muir and R. J. LaBauve)

Work continues on the development of benchmark specifications for the ZPPR/FTR-2 shield experiment performed by Argonne National Laboratory.[8,9] A previous paper[10] described our analysis of the
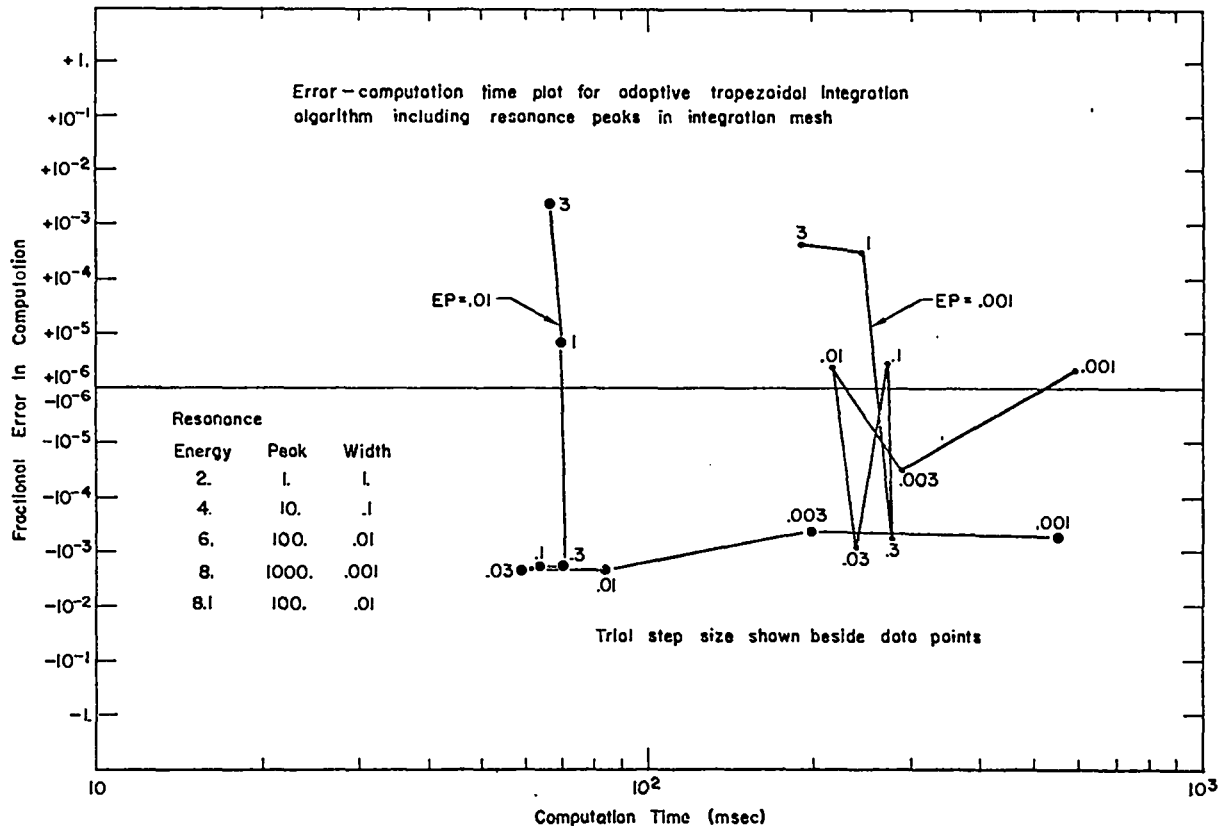
Fig. 2. Error-computation time plot for adaptive trapezoidal integration
algorithm including resonance peaks in integration mesh.

ZPPR/FTR-2 neutron reaction rate measurements. We have now completed an analysis of the gamma-ray portion of that experiment in which ^{7}LiF thermoluminescent dosimeters (TLD's) were distributed throughout the core, reflector, and shield segment of the ZPPR/FTR-2 assembly. The 3mm X 3mm X 0.9mm ribbons were not encased in electron-equilibrium sleeves, but were surrounded on all sides by at least 0.4mm of stainless steel (structural and canning material). The response of the TLD's has been calculated previously,[11] but in that calculation gamma-ray production by inelastic scattering was ignored and corrections were not applied for either cavity-ionization or fast-neutron effect.

The gamma-ray source distribution was constructed using the neutron flux distribution calculated previously.[10] The prompt gamma-ray production cross sections were derived from ENDF/B-III using LAPHANO[12] in the commonly-used pointwise mode. That is, the resonance parameters from ENDF/B were removed by a preprocessor and the resulting pointwise file pro-

cessed by LAPHANO, using a fine-group neutron weighting function produced by MC^2.[13] Fission product gamma-ray spectra are not yet available in ENDF/B, so the data given in Ref. 11 were used for this component. Multigroup photon interaction cross sections were obtained by processing ENDF/B photon evaluation data[14] with the GAMLEG[15] code. The gamma-ray flux distribution was calculated using the two-dimensional discrete ordinates code TWOTRAN[16] in the P_2S_6 approximation.

An absolute comparison of the TLD responses measured and calculated along the reactor midplane are given in Fig. 3. The lower calculated curve was obtained using a gamma-ray flux-to-dose conversion factor[17] which ignores the enhancement of TLD sensitivity due to the adjacent high-Z materials (steel). The middle curve shows the enhanced response produced by including an approximate treatment of the steel environment. This correction is based on a cavity-ionization-theory calculation performed by Yule and Simons.[18] The upper curve
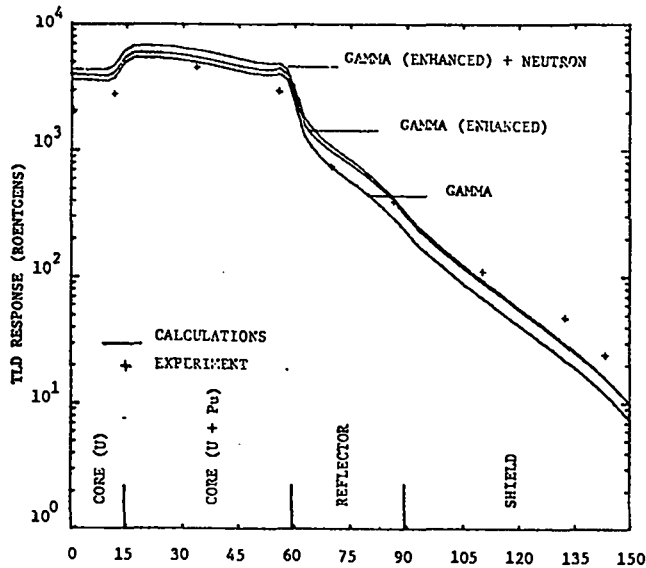
Fig. 3. Measured and calculated TLD response
in ZPPR/FTR-2 for a central traverse.

includes, in addition, an estimate of the effect of
fast neutron interactions in the TLD material.[19] The
uncertainty in the magnitude of these two corrections,
as well as the systematic effects which have not been
included, lead to a combined uncertainty of about 15%
in the ratio of calculation to experiment.

The agreement between calculation and experiment
is generally quite good. The largest discrepancy,
about a factor of two, is in the center of the de-
pleted-uranium section at the center of the core.
Most of this difference can be attributed to the use
of LAPHANO in the pointwise mode, since this does not
allow for self-shielding of the large ^{238}U capture
resonances. Comparisons of the ^{238}U capture cross
section calculated using MC^2 with the LAPHANO results
indicate that calculated values in the depleted re-
gion should be lowered by about the required factor
of two. Self-shielding effects are not large in the
reflector and shield regions because the neutron mul-
tigroup structure is fairly fine (lethargy width of
0.25) in the region of the large Fe and Ni scatter-
ing resonances. The discrepancy at large radii is
due to undercalculation of the neutron flux, as
shown by the results for the ^{239}Pu fission traverse
discussed in Ref. 10.

IV. TRANSPORT OF THERMONUCLEAR NEUTRONS IN HOT HY-
DROGEN (D. R. Harris, J. M. Wallace [TD-1],
and W. B. Wilson [Texas A&M])

The violent motions of scattering nuclei affect
the transport of neutrons in a nuclear burn.
We have examined these transport effects in multi-
group nuclear design methods by: a) calculation of
multigroup cross-section sets for hot target nuclei
with and without a superimposed translational velo-
city; b) multigroup S_n calculation of neutron
fluxes emerging and reflected from hot hydrogen
shells enclosing a thermonuclear source.

Simple translational motion of target nuclei
can, at least in principle, be treated by kinematic
modifications of S_n and multigroup Monte Carlo mod-
ules. Thermal motions of target nuclei are most
simply treated, however, by providing these modules
with multigroup cross-section sets computed for tar-
get nuclei at relevant temperatures. We have calcu-
lated multigroup cross-section sets for hot target
nuclei using the PLINY2 code. This code executes
by Monte Carlo techniques the required multiple in-
tegrals over direction and speed of the target nu-
clei, over energy of the incident particle, over
scattering angles and energy of the emitted particle
in the center-of-mass frame, and over direction and
energy of the emitted particle after transformation
back to the lab frame.[20] Figure 4 illustrates cross
sections and sampling uncertainties for group-to-
group transfer of neutrons colliding with hydrogen
at various temperatures.

Figure 5 shows the spectra of neutrons emerging
from hot hydrogen shells at various temperatures,
all at liquid hydrogen density and extending from
radius 10-cm to radius 11-cm around a D-T source.
These calculations were made using the DTF-IV code[21]
in a standard 30 multigroup structure. Figure 6
shows the effect on the emerging neutron spectrum
of superimposing a translational velocity at 1% of
the speed of light on a 10^9°K hydrogen shell. Fig-
ure 7 shows the neutron flux spectrum reflected back
toward the burn as well as the spectrum emerging
from the outside of hot (10^9°K) and cold (0°K) hy-
drogen shells. These figures exhibit substantial
effects on transport of neutrons with energies near
the average energy of the thermal motion.

5
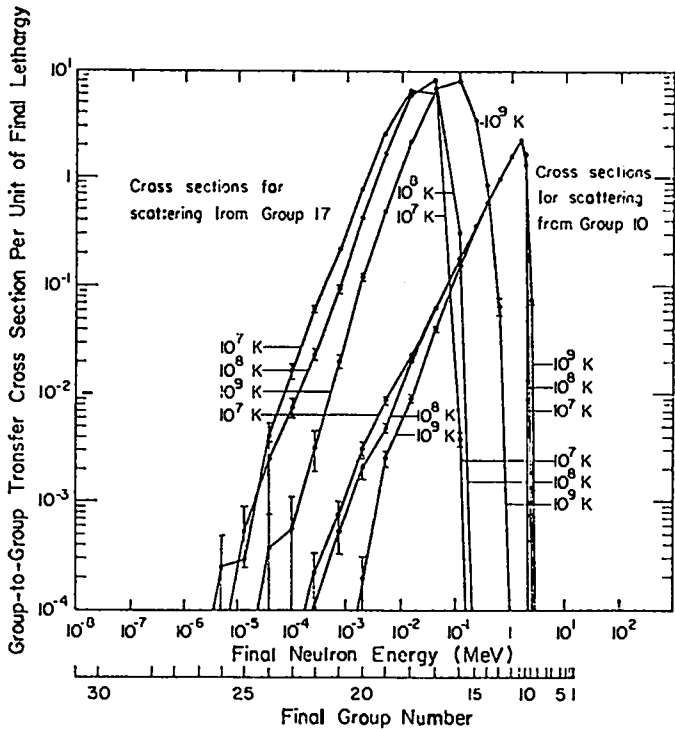
Fig. 4. Cross sections for hot hydrogen scattering from groups 10 and 17 to final groups (per unit final lethargy).
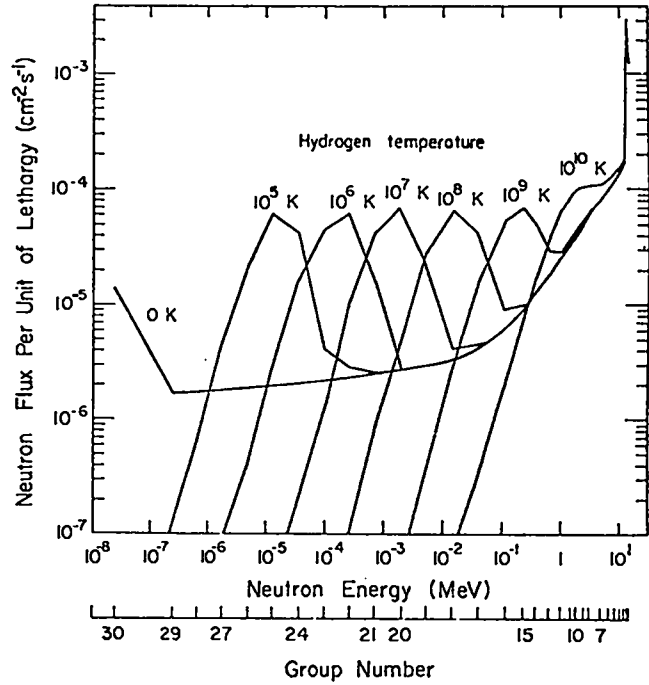
Fig. 5. Neutron spectra emerging from a 1-cm-thick hydrogen shell at various temperatures. The hydrogen shell has inner radius 10-cm and encloses a D-T neutron source in vacuum.
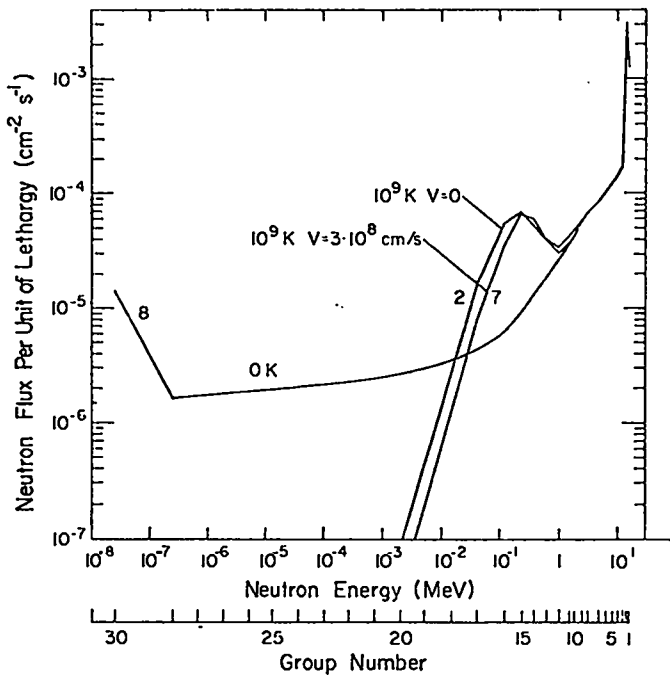
Fig. 6. Neutron spectra emerging from a cold hydrogen shell and from a hot hydrogen shell with and without an outward translation at 1% of the speed of light.
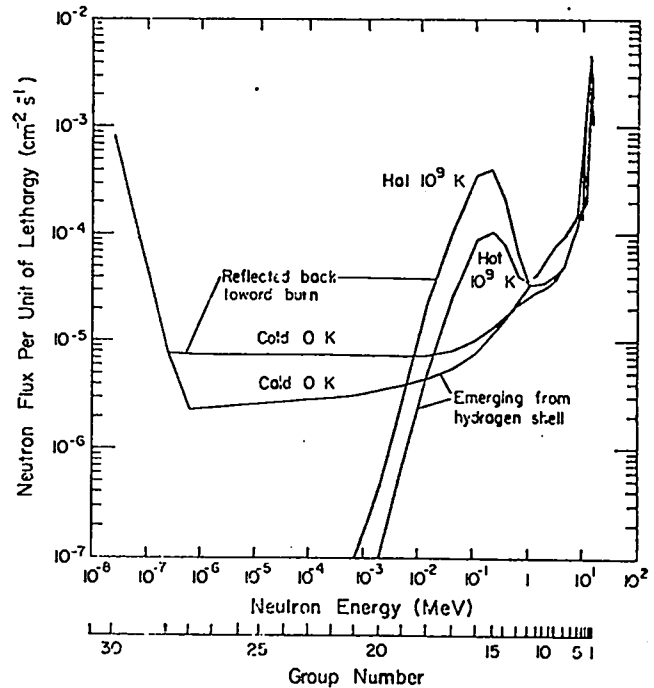
Fig. 7. Neutron spectra emerging from and reflected from hot and cold hydrogen shells. Each hydrogen shell encloses a D-T source in low-density hydrogen.

6

V. ENDF/B-IV DELAYED NEUTRON PRECURSORS AND CALCU-
    LATED YIELDS PER FISSION (T. R. England)

Table I lists data for 57 delayed neutron pre-
cursors to be included in the ENDF/B-IV decay files.
As a group, the delayed precursors are particularly
sensitive to the parameters used in the charge dis-
persion model because the average precursor is ~ 1
charge unit on the neutron rich side of the empiri-
cal Gaussian distribution. The sensitivity is noted
in Table II.

Calculations of delayed neutrons per fission
have been made using all 10 yield sets of ENDF/B-IV.
Table III lists the results by the conventional 6
group totals and the aggregate values over all groups.
The ordered contributions of each nuclide, based on
^{235}U thermal calculations using ENDF/V-IV data, is
given in Table IV.

The remaining tables, except for experimental
values in Table XIII, are calculational results using
ENDF/B-IV mass yield data and/or the charge distri-
bution fractional yields, where

$$Y \equiv \text{Mass chain yield}$$

$$FCY \equiv \begin{array}{l}\text{Cumulative precursor yield fraction}\\\text{of Y}\end{array}$$

$$\sum P_n * Y = \begin{array}{l}\text{Neutron emission based on total chain}\\\text{yield to precursor}\end{array}$$

$$\sum P_n * FCY = P_n \text{ weighted by precursor yield fraction}$$
$$\sum P_n * FCY * Y = \text{Delayed neutron emission.}$$

Table V - Results based only on ENDF/B-IV data.

Table VI - compares calculated values using model
    FCY's and FCY's from ENDF/B-IV. (Note: The
    fast and thermal d.n. yields should be nearly
    constant. The use of model values for FCY show
    this, but results are low. As noted below, in
    Tables VII and VIII, the removal of the even-
    odd factor significantly increased model esti-
   mates.)

Table VII - Six group values using model FCY's and
    even-odd Z factor = 25%.

Table VIII - Same as Table VII with removel of even-
    odd Z factor.

Table IX - ^{235}U at 14.6 MeV, no even-odd Z factor,
    model FCY.

Table X - ^{239}Pu fast and thermal values using model
    FCY's.

Table XI - ^{238}U fast, no even-odd Z effect, model
    · FCY's.

Table XII - ^{233}U thermal with even-odd Z factor,
    model FCY's.

Table XIII - Some comparison experimental d.n.y.'s
    and preliminary ENDF/B-IV evaluations.

Except where otherwise labeled, the above tables
use FCY values calculated using the charge dispersion
model at LASL,[*] the even-odd Z factor is 1.25 (1.15
for ^{235}U at 14.6 MeV and 1.0 for ^{239}Pu). ENDF/B-IV
yields use the same model except for the even-odd Z
factor where a compromise value of 1.20 is used for
all energies and all nuclides. In addition, ENDF/B-
IV uses experimental values of fractional yields
where available, combined with model values.

COMMENT: For the fissile nuclides the experi-
mental d.n.y. values are essentially constant up to
second chance fission (neutron energies of ~ 4 to 5
MeV). ENDF/B-IV data yields d.n.y. values for all
fast and 14-MeV fission which are markedly low.
This strongly indicates that fast spectrum yields to
d.n. precursors are in error. The use of FCY values
from the empirical charge dispersion model with or
without the even-odd Z factor provide nearly con-
stant d.n.y. vs. the fission neutron energy, in qual-
itative agreement with experiment. In addition, re-
moval of the even-odd Z effect provides excellent
quantitative agreement for fast and thermal d.n.y.
values, except for ^{238}U. There is no reason to ex-
pect the empirical FCY model to provide better a-
greement with experiment than does ENDF/B-IV; how-
ever, these results do suggest that the independent
yields in fast neutron fission are too low, that the
even-odd Z factor may not apply even in thermal ^{235}U
fission for delayed neutron precursors, and that
chain yields for ^{238}U fission require improvement.

---

[*]LASL uses the basic Wahl et al model outlined in
LASL internal memorandum T-2-L-600, 6/5/73, plus
attachments, and with even-odd Z factors as summa-
rized in LASL internal memorandum T-2-L-816,
12/19/73. Where chain data is sufficient, Terrell's
summation method (Phys. Rev. 127, 880, 1962) is
used in determination of $Z_p(A)$. Fractional yields
have been computed and will be issued shortly as
LA-5553-MS by K. Wolfsberg. Results will differ
from ENDF/B-IV because of use of different even-
odd Z factors and incorporation of experimental
values in the ENDF/B evaluation. Rider will pub-
lish the ENDF/B values. It differs from the model
as noted in LASL internal memorandum T-2-L-885,
2/7/74.

TABLE I
DELAYED NEUTRON EMISSION PROBABILITIES (Pn)*

Delayed Group	Precursor	Q_β	B_n	$(Q_\beta - B_n)$	Pn %	$T_{1/2}$ (sec)
4	$^{79}Ga_{31}$	6.06	5.70	0.36	(0.14)	2.86±0.04
4	$^{80}Ga_{31}$	9.44	8.50	0.94	(0.86)	1.7±0.2
4	$^{83}Ge_{32}$	8.49	8.11	0.38	(0.16)	1.9±0.4
4	$^{84}Ge_{32}$	7.54	4.15	3.39	(9.6)	1.2±0.3
3	$^{84}As_{33}$	9.99	9.06	0.93	0.13±0.06	5.8±0.4
4	$^{85}As_{33}$	9.05	4.10	4.95	20.±4.0	2.03±0.01
5	$^{86}As_{33}$	11.35	6.22	5.13	$3.8^{+1.7}_{-1.0}$	0.9±0.2
6	$^{87}As_{33}$	10.41	4.11	6.3	(31)	0.3±0.2
3	$^{87}Se_{34}$	7.27	6.40	0.87	0.18±0.03	5.6±0.1
4	$^{88}Se_{34}$	6.33	4.85	1.48	0.5±0.3	1.5±0.1
5	$^{89}Se_{34}$	8.63	6.15	2.43	5.0±1.5	0.41±0.04
1	$^{87}Br_{35}$	6.68	5.46	1.22	2.3±0.02	55.7±0.11
2	$^{88}Br_{35}$	8.98	7.15	1.83	4.6±0.4	15.9±0.2
3	$^{89}Br_{35}$	8.04	5.22	2.82	8.6±0.9	4.5±0.1
4	$^{90}Br_{35}$	10.33	6.21	4.12	12.±3.	1.6±0.1
5	$^{91}Br_{35}$	9.18	4.57	4.61	$7.^{+10.}_{-4.}$ (C)	0.6±0.1
6	$^{92}Br_{35}$	12.01	6.21	5.80	(26.)	0.3±0.1
4	$^{92}Kr_{36}$	5.31	5.06	0.25	0.040±0.007	1.84±0.02
4	$^{93}Kr_{36}$	8.15	6.30	1.85	3.2±0.06	1.27±0.02
6	$^{94}Kr_{36}$	6.56	4.33	2.23	(4.4)	0.21±0.02
3	$^{92}Rb_{37}$	7.78	7.35	0.43	0.012±0.004	4.53±0.03
3	$^{93}Rb_{37}$	6.62	5.14	1.48	1.62±0.23	5.8±0.1
4	$^{94}Rb_{37}$	9.45	7.17	2.28	11.1±1.0	2.69±0.04
5	$^{95}Rb_{37}$	7.87	4.64	3.23	7.10±0.93	0.36±0.02
6	$^{96}Rb_{37}$	10.76	6.62	4.14	12.7±1.5	0.207±0.006
6	$^{97}Rb_{37}$	9.03	3.92	5.11	(21.)	0.17±0.01
6	$^{98}Rb_{37}$	12.11	6.39	5.72	(26.)	0.14±0.01
6	$^{99}Rb_{37}$	10.07	3.09	6.98	(37.)	0.076±0.005
6	$^{97}Sr_{38}$	7.10	6.81	0.29	(0.095)	0.2±0.2
5	$^{98}Sr_{38}$	5.37	4.67	0.70	(0.50)	0.85±0.005
4	$^{97}Y_{39}$	5.35	5.22	0.13	1.6±0.3 (C)	1.11±0.03
6	$^{98}Y_{39}$	8.24	7.55	0.69	(0.48)	0.3±0.01

TABLE I (Cont.)

Delayed Group	Precursor	Q_β	B_n	$(Q_\beta - B_n)$	Pn %	$T_{1/2}$ (sec)
5	$^{99}Y_{39}$	6.51	4.44	2.07	(3.8)	0.8±0.7
4	$^{127}In_{49}$	6.37	5.55	0.82	(0.67)	2.0±0.4 +
3	$^{128}In_{49}$	8.42	7.79	1.13	(1.2)	3.7±0.5
5	$^{129}In_{49}$	7.31	5.32	1.99	(3.5)	0.8±0.3
5	$^{130}In_{49}$	9.69	7.42	2.27	(4.5)	0.5±0.2
6	$^{131}In_{49}$	8.39	5.02	3.37	(9.5)	0.3±0.1
4	$^{133}Sn_{50}$	7.24	7.11	0.13	(0.021)	1.47±0.4
2	$^{134}Sb_{51}$	8.69	7.35	1.34	0.08±0.02	11.3±0.3
4	$^{135}Sb_{51}$	7.52	3.86	3.66	8.±2.	1.70±0.02
2	$^{136}Te_{52}$	4.47	4.02	0.45	-0.5	21.±1.
3	$^{137}Te_{52}$	6.48	5.63	0.85	~0.5	3.5±0.5
2	$^{137}I_{53}$	5.79	4.45	1.34	5.4±1.3	24.6±0.2
3	$^{138}I_{53}$	7.80	5.86	1.94	2.5±0.5	6.5±0.1
4	$^{139}I_{53}$	6.67	3.89	2.78	10.±3.	2.4±0.1
5	$^{140}I_{53}$	8.93	5.35	3.58	32.±13.	0.86±0.04
5	$^{141}I_{53}$	7.42	3.52	3.90	(12.)	0.4±0.1
4	$^{141}Xe_{54}$	5.85	5.79	0.06	0.054±0.009	1.72±0.01
4	$^{142}Xe_{54}$	4.34	3.92	0.42	0.51±0.09	1.22±0.02
6	$^{143}Xe_{54}$	6.65	5.59	1.06	(1.1)	0.30±0.25
2	$^{141}Cs_{55}$	4.97	4.65	0.32	0.073±0.011	25.0±0.3
4	$^{142}Cs_{55}$	7.24	6.20	1.04	0.21±0.06	1.7±0.1
4	$^{143}Cs_{55}$	5.73	4.09	1.64	1.13±0.025	1.7±0.1
4	$^{144}Cs_{55}$	8.05	6.16	1.87	1.10±0.25	1.02±0.04
5	$^{145}Cs_{55}$	6.07	3.83	2.24	(4.4)	0.56±0.03
6	$^{146}Cs_{55}$	8.54	6.45	2.09	(3.9)	0.19±0.01

+ $^{127}In_{49}$ has an isomeric state with $T_{1/2}$ = 3.64 ± 0.04 sec.

*57 nuclides in the order listed in L. Tomlinson, Atomic and Nuclear Data Tables 12, 179-194 (1973).

All Q_β and B_n values based on G. T. Garvey et al, Rev. Mod. Phys. 41, S1 (1969). Pn's in () are very approximate; they are derived from $P_n = 0.97 (Q_\beta - B_n)^{1.88}$. (Fit to 33 values.)

All other values are from L. Tomlinson, Atomic and Nuclear Data Tables 12, 179-194 (1973); values followed by "C" are calculated from delayed neutrons per fission and precursor yields.

Half-lives, where available, were taken from the GE Chart of the Nuclides, 11th Ed. Revised to April 1972. Uncertainties were taken from the preliminary ENDF/B decay data tape 970. In the few cases where these sources had only estimated data, half-lives from Tomlinson's compilation were used.

TABLE II

SENSITIVITY OF PRECURSOR YIELDS TO
SOME YIELD MODEL PARAMETERS

Quantity		Comment
$Z-Z_p$	–	For $Z-Z_p = -1.0$, a variation of 0.1 charge units varies the FCY by ~ 26% (Specifically, FCY = $0.186^{+0.052}_{-0.044}$)
Even-Odd Z Effect*	–	For $Z-Z_p = -1.1$ (average), an assumed 25% effect decreases the calculated delayed neutron yield from 1.68 to 1.33 (^{235}U thermal) or ~ 26%.
Gaussian σ	–	At $Z-Z_p = -1.0$, a $\sigma = 0.56 \pm 0.06$ varies FCY by ~ ± 13% (Specifically, FCY = $0.186^{+0.025}_{-0.024}$)

---

*A 25% effect means the fractional independent (direct) yields estimated from the Gaussian distribution are increased 25% for even Z and decreased 25% for odd Z.

TABLE III

DELAYED NEUTRON YIELDS PER 100 FISSIONS
USING ONLY ENDF/B-IV NUCLIDE FISSION YIELDS
(57 PRECURSORS)

APPROX. GROUP	U235T	U235F	U235HE	U238F	U238HE	PU239T	PU239F	PU241T	U233T	Th232F
1	0.0506	0.0439	0.0446	0.0397	0.0380	0.0179	0.0115	0.0154	0.0531	0.1412
2	0.3035	0.2423	0.1503	0.4273	0.1969	0.1640	0.1067	0.2375	0.2201	0.5374
3	0.2697	0.1817	0.2259	0.3750	0.2275	0.0659	0.0388	0.1174	0.1528	0.5240
4	0.6209	0.4383	0.5763	1.1181	0.6792	0.2078	0.1130	0.3614	0.3118	1.1572
5	0.2568	0.1582	0.1679	0.8751	0.4167	0.0873	0.0411	0.2015	0.0482	0.4260
6	0.0722	0.0403	0.0607	0.2524	0.1533	0.0206	0.0093	0.0488	0.0163	0.1668
TOTAL	1.5738	1.1046	1.2256	3.0875	1.7115	0.5634	0.3203	0.9820	0.8024	2.9527
	(1.463)*	(1.030)*	(1.138)*	(2.690)*	(1.492)*	(0.504)*	(0.290)*	(0.870)*	(0.769)*	(2.749)*

*Totals Before Using Fitted Pm's Noted in TABLE I

TABLE IV

ORDERED LIST OF DELAYED NEUTRON EMISSION
PER 100 FISSIONS FOR ^{235}U THERMAL FISSION
(Calculated using ENDF/B-IV Data)

Group	Nuclide	D.N./100 Fissions	% of TOT	Group	Nuclide	D.N./100 Fissions	% of TOT
4	$^{94}Rb_{37}$	.2065	13.12	2	$^{141}Cs_{55}$	.0032	0.20
2	$^{137}I_{53}$	.1757	11.16	4	$^{144}Cs_{55}$	.0031	0.20
3	$^{89}Br_{35}$	.1673	10.63	5	$^{145}Cs_{55}$	.0030	0.19
4	$^{90}Br_{35}$	.1579	10.03	5	$^{98}Sr_{38}$	.0029	0.18
2	$^{88}Br_{35}$	.1154	7.33	5	$^{130}In_{49}$	.0029	0.18
4	$^{97}Y_{39}$	.0791	5.03	6	$^{131}In_{49}$	.0022	0.14
4	$^{139}I_{53}$	.0752	4.78	3	$^{137}Te_{52}$	.0021	0.13
5	$^{140}I_{53}$	.0724	4.60	4	$^{142}Xe_{54}$	.0020	0.13
5	$^{99}Y_{39}$	.0697	4.43	3	$^{87}Se_{34}$	.0018	0.11
5	$^{95}Rb_{37}$	.0630	4.00	4	$^{88}Se_{34}$	.0017	0.11
3	$^{93}Rb_{37}$	.0566	3.60	6	$^{97}Y_{38}$	.0017	0.11
1	$^{87}Br_{35}$	.0506	3.22	4	$^{84}Ge_{32}$	.0015	0.10
3	$^{138}I_{53}$	.0403	2.56	5	$^{129}In_{49}$	.0012	0.08
4	$^{85}As_{33}$	.0360	2.88	6	$^{98}Rb_{37}$	.00098	0.06
5	$^{91}Br_{35}$	.0297	1.89	4	$^{141}Xe_{54}$	.00066	0.04
6	$^{87}As_{33}$	.0217	1.38	3	$^{128}In_{49}$	.00064	0.04
4	$^{143}Cs_{55}$	.0175	1.11	4	$^{92}Kr_{36}$	.00062	0.04
4	$^{93}Kr_{36}$	.0166	1.05	3	$^{92}Rb_{37}$	.00058	0.04
6	$^{98}Y_{39}$	.0163	1.04	6	$^{143}Xe_{54}$	.00056	0.04
4	$^{135}Sb_{51}$	.0160	1.02	3	$^{84}As_{33}$	.00038	0.02
6	$^{94}Kr_{36}$	.0116	0.74	2	$^{134}Sb_{51}$	.00037	0.02
2	$^{136}Te_{52}$	.0089	0.57	4	$^{127}In_{49}$	.00029	0.02
6	$^{97}Rb_{37}$	.0070	0.44	6	$^{146}Cs_{55}$	.00029	0.02
4	$^{142}Cs_{55}$	.0058	0.37	4	$^{80}Ga_{31}$	.00017	0.01
6	$^{96}Rb_{37}$	.0051	0.32	4	$^{83}Ge_{32}$	.00014	0.009
6	$^{92}Br_{35}$	.0047	0.30	6	$^{99}Rb_{37}$	.00007	0.004
5	$^{89}Se_{34}$	.0044	0.28	4	$^{133}Sn_{50}$	.00003	0.002
5	$^{86}As_{33}$	.0039	0.25	4	$^{79}Ga_{31}$	.00002	0.001
5	$^{141}I_{53}$	.0037	0.24				

TABLE V

AGGREGATE VALUES OF P_n TIMES MASS YIELDS [a]
AND FRACTIONAL YIELDS - ENDF/B-IV DATA

Nuclide	$\sum P_n * Y$	$\sum P_n * FCY$	d.n.y. $\sum P_n * FCY*/100$ Fiss	d.n.y. FCY Model Even-Odd Z Factor = 1.0
U235T	17.53	32.54	1.574	1.676
U235F	17.04	23.55	1.105	1.648
U235HE	14.91	31.18	1.226	1.166
U238F	15.13	77.92	3.088	3.280
U238HE	13.88	50.23	1.711	--
Pu239T	13.88	16.06	0.5634	.574
Pu239F	13.46	8.63	0.3203	.574
Pu241T	12.63	34.14	0.9820	--
U233T	18.36	14.62	0.8024	--
TH232F	19.42	50.68	2.953	--

TABLE VI

Comparison Results Using ENDF/B-IV and Model Values
for FCY (^{235}U, with even-odd Z factor = 25%)

Energy	$\sum YXP_n$	$\sum (FCY)XP_n$ ENDF	$\sum (FCY)XP_n$ Model	d.n.y. $\sum YX(FCY)XP_n$ ENDF	d.n.y. $\sum YX(FCY)XP_n$ Model	$\sum \frac{(z-z_p)}{57}$
Thermal	17.532	32.537	28.096	157.35	132.64	-1.095
Fast	17.037	23.550	29.312	110.46	135.67	-1.138
% Decrease from Thermal	2.8	27.6	-4.3	29.8	-2.3	

TABLE VII

^{235}U, EVEN-ODD Z EFFECT = ± 25% [b]

Group	$\sum P_n * Y$ Thermal	$\sum P_n * Y$ Fast	$\sum P_n * FCY$ Thermal	$\sum P_n * FCY$ Fast	d.n.y. $\sum P_n * FCY*Y$ Thermal	d.n.y. $\sum P_n * FCY*Y$ Fast	$\sum \frac{(z-z_p)}{57}$ Thermal	$\sum \frac{(z-z_p)}{57}$ Fast
1	5.856	5.561	1.976	1.992	5.030	4.816	-1.101	-1.075
2	54.678	54.051	5.633	5.693	28.055	28.013		
3	73.368	69.678	3.703	4.523	18.412	22.333		
4	345.306	333.007	11.772	12.005	54.332	53.930		
5	444.322	433.093	3.803	3.857	20.747	20.409		
6	829.716	808.360	1.209	1.242	6.066	6.164		
	1753.246	1703.750	28.096	29.312	132.643	135.665		

---

[a] d.n.y. = delayed neutron yield. In Table V d.n.y. is per 100 fissions and on the following tables per 10,000 fissions.

[b] FCY from model using even-odd Z effect of ± 25% except where otherwise noted. All d.n.y. calculations use ENDF/B-IV mass chain yields.

TABLE VIII

^{235}U NO EVEN-ODD Z EFFECT [a]

Group	$\sum P_n*Y$ Thermal	$\sum P_n*Y$ Fast	$\sum P_n*FCY$ Thermal	$\sum P_n*FCY$ Fast	$\sum P_n*FCY*Y$ d.n.y. Thermal	$\sum P_n*FCY*Y$ d.n.y. Fast	$\dfrac{\sum(z-z_p)}{57}$ Thermal	$\dfrac{\sum(z-z_p)}{57}$ Fast
1	5.856	5.561	2.047	2.059	5.212	4.977	-1.101	-1.075
2	54.678	54.051	6.489	6.544	32.410	32.298		
3	73.368	69.678	4.797	5.630	23.629	27.608		
4	345.306	333.007	14.579	14.968	66.608	66.781		
5	444.322	433.093	4.830	4.904	26.350	25.978		
6	829.716	808.360	1.512	1.436	13.434	7.047		
	1753.246	1703.750	34.255	35.541	167.643	164.780		

TABLE IX

^{235}U, 14.6 MeV, No Even-Odd Z Effect [a]

Group	$\sum P_n*Y$	$\sum P_n*FCY$	$\sum P_n*FCY*Y$ d.n.y.	$\dfrac{\sum(z-z_p)}{57}$
1	6.185	2.084	5.603	-1.303
2	45.197	4.504	16.865	
3	61.180	5.205	22.203	
4	282.638	13.532	50.229	
5	356.115	3.423	16.117	
6	739.677	1.277	5.609	
	1490.991	30.025	116.626	

TABLE X

^{239}Pu No Even-Odd Z Effect [a]

Group	$\sum P_n*Y$ Thermal	$\sum P_n*Y$ Fast	$\sum P_n*FCY$ Thermal	$\sum P_n*FCY$ Fast	$\sum P_n*FCY*Y$ d.n.y. Thermal	$\sum P_n*FCY*Y$ d.n.y. Fast	$\dfrac{\sum(z-z_p)}{57}$ Thermal	$\dfrac{\sum(z-z_p)}{57}$ Fast
1	2.201	2.498	1.523	1.518	1.457	1.648	-1.456	-1.442
2	46.799	44.789	3.906	4.135	16.896	17.686		
3	39.803	41.772	2.493	2.462	7.203	7.674		
4	242.859	239.166	5.417	5.427	21.155	19.820		
5	363.167	351.524	1.769	1.798	8.884	8.571		
6	693.216	666.719	0.348	0.334	1.772	1.610		
	1388.045	1346.467	15.455	15.674	57.366	57.010		

---

[a] FCY from model, yields ENDF/B-IV

TABLE XI

^{238}U, No Even–Odd Z Effect[a]

Group	$\sum P_n * Y$	$\sum P_n * FCY$	d.n.y. $\sum P_n * FCY * Y$	$\dfrac{\sum (z - z_p)}{57}$
1	4.050	2.233	3.933	−0.635
2	47.478	9.429	42.198	
3	51.124	9.959	35.579	
4	272.122	33.198	122.200	
5	397.164	19.617	96.443	
6	740.642	6.938	27.941	
	1512.580	81.374	328.294	

TABLE XII

^{233}U, Even–Odd Z Effect = 25%[a]
(Thermal)

Group	$\sum P_n * Y$	$\sum P_n * FCY$	d.n.y. $\sum P_n * FCY * Y$
1	9.212	1.555	6.227
2	66.364	2.797	16.759
3	85.196	2.160	13.438
4	382.262	4.912	24.628
5	469.337	1.092	5.711
6	824.078	0.311	1.628
	1836.448	12.828	68.391

TABLE XIII

DELAYED NEUTRONS/100 FISSIONS
SOME EXPERIMENTAL + EVALUATED VALUES

Nuclide	Keepin Fiss Spec	Krick & Evans AVE 0.1--1.8 MeV	Masters 3.1 MeV	ENDF/B–IV Preliminary 10^{-5}ev--4.0 MeV
^{235}U	1.65 ± 0.07	1.63 ± 0.13	1.72 ± 0.13	1.67
^{238}U	4.12 ± 0.25	----	4.84 ± 0.36	4.60
^{239}U	0.63 ± 0.05	0.62 ± 0.05	0.66 ± 0.05	0.645
^{233}U	0.70 ± 0.06	0.75 ± 0.06	0.74 ± 0.06	----
^{232}Th	4.96 ± 0.35	----	5.7 ± 0.5	----

[a] FCY from model, mass yields from ENDF/B–IV

VI. ENDF/B-IV DECAY FILES   (T. R. England)

A.   General Content

Table XIV summarizes the expected content regarding the number of nuclides and type of parameters.

B.   Nuclide Fission Yields

The 10 yield sets noted in Table XIV are complete. Some Phase I reviews are still in progress.

During the ENDF/B-IV Fission Product Task Force Meeting at HEDL April 8-9, 1974, Bill Maeck and Bill McElroy presented evidence that neodymium yields in ENDF/B-IV for ^{239}Pu fast neutron fission were low by ~ 4 to ~ 7%. These yields are particularly important in analysis of fuel depletion, and also to absorption in thermal reactors. We also found that a change to the recommended values of Table XV would improve the normalization (current 199.51 to 200.25%) and would therefore not require other changes in the heavy mass yields. In view of the uncertainties in fast ^{239}Pu yields, and their probable energy dependence, there was no objection to recommended changes.

In addition, it is necessary to have a standard reference in fuel analysis. We therefore recommend:

1. ENDF/B-IV yields should be used as the standard reference in fuel analysis.

2. If time permits, the independent yields in ^{239}Pu fast neutron fission should be increased by the ratios in Table XVI for the indicated mass numbers.

A LASL code was prepared to examine some aspects of the yields in ENDF/B form, including delayed neutron calculations. Table XVIII gives the overall yield summation per set. These are not precisely 200%; the sums match the expected values.

K. Wolfsberg has provided the $\bar{\nu}$ values calculated from the mass chain yields using Terrell's summation method in Table XVIII.

The final ENDF/B-IV yields vs. charge used a normal distribution about a $Z_p(A)$ modified by an even-odd Z factor. The $Z_p(A)$'s were provided by LASL. The even-odd Z factor appears to be supported by independent yields for ^{235}U + n_{th} fission and is expected to be larger for thermal than high energy fissions. It has not been demonstrated that the factor applies to other nuclides and, in particular, to ^{239}Pu fast fission. The factor likely differs with fissionable nuclides and neutron energy; however, a single compromise value of ± 1.20 was used in ENDF/B-IV. Where yield fractions are known these are used, but dispersion model values were not entirely discarded. The actual ENDF/B value is an inverse variance weighting of measured and model values. However, the 1 σ uncertainty assigned to the model value depended on the absolute yield, not to the Z_p, σ, and even-odd Z effect. In particular, when the absolute yield was > 1%, 1/2 $\leq$ to < 1% and < 1/2%, the uncertainties assigned to the model values were ± 32%, ± 64%, and ± 100% respectively. Where only the model values are available, these uncertainties will often be too small. The weighted independent yields are added and normalized to the total Z chain yield for the final yield set per isobaric chain.

For isomeric states, independent yields from the model are split evenly between states; measure values for a given fission process are incorporated as noted above where they are known. This is one area that must be improved in future files, and the entire dispersion model certainly requires improvement, especially for fission other than ^{235}U + n_{th}.

TABLE XIV

FISSION PRODUCT FILES GENERAL CONTENT

1.
Number	Type, Comment
825	Total Decay/Absorption File
712	Unstable
~ 701	Ground State
~ 117	1st Excited State ($\tau_{1/2} > 0.1$ sec)
7	2nd Excited State ($\tau_{1/2} > 0.1$ sec)
113	Stable (includes some α decay for $\tau_{1/2} > 10^{10}$ years)
57	Delayed Neutron Precursors (have P_n values)
6	α Decay ($\tau_{1/2} > 10^{10}$ years)
17	β+
182	Line Data (γ energies and intensities and β end point energies)
~ 175	σ(E), 10^{-5}<eV→20 MeV

Average β^+, α and total γ-decay energies included for all unstable nuclides.

2. Yields (Masses 72→167, Charges 26→70). 1019 independent yields for each of the following:

Fissionable Nuclide	Thermal	Fast	~ 14 MeV
^{235}U	X	X	X
^{238}U		X	X
^{239}Pu	X	X	
^{241}Pu	X	X	
^{233}U	X		
^{232}Th		X	

NOTE: Yields will be in usual file for each fissionable nuclide. Decay and cross section files (f457) will be together for fission products (3 to 4 magnetic tapes). Decay files include Q values and branching fractions.

3. Non-fission products. Decay data in general purpose file includes, but is not limited to, the following 18 nuclides: ^{3}H, ^{187}Re, ^{232}Th, ^{233}Pa, 233, 234, 235, 236, ^{238}U, ^{237}Np, 238, 239, 240, 241, ^{243}Am, and ^{244}Cm.

TABLE XV			TABLE XVI	
RECOMMENDED ^{239}Pu Nd YIELDS IN FAST NEUTRON FISSION			RATIO OF NEW TO CURRENT INDEPENDENT ENDF/B-IV YIELDS IN ^{239}Pu FAST NEUTRON FISSION	

TABLE XV

RECOMMENDED ^{239}Pu Nd YIELDS
IN FAST NEUTRON FISSION

Nuclide	% Yield (± 3%)
^{143}Nd	4.46
^{145}Nd	3.08
^{146}Nd	2.54
^{148}Nd	1.72
^{150}Nd	1.03

TABLE XVI

RATIO OF NEW TO CURRENT INDEPENDENT
ENDF/B-IV YIELDS IN ^{239}Pu FAST NEUTRON FISSION

Mass	Ratio
143	4.46/4.1588
145	3.08/2.8985
146	2.54/2.4021
148	1.72/1.6388
150	1.03/0.99314

TABLE XVII

CUMULATIVE YIELD SUMMATION IN ENDF/B-IV

Nuclide	Energy	Sum to sym Fission	All A
^{235}U	T	100.03	200.04
^{235}U	F	100.14	200.07
^{235}U	HE	102.30	200.36
^{238}U	F	100.05	200.10
^{238}U	HE	101.77	199.85
^{239}Pu	T	100.12	200.10
^{239}Pu	F	99.89	199.51*
^{241}Pu	T	99.48	198.48
^{233}U	T	99.76	199.51
^{232}Th	F	100.05	200.13

*This would change to 200.25 using the
recommended Nd yields.

TABLE XVIII

CALCULATED $\bar{\nu}$ FROM MASS YIELDS[a]

	$\bar{\nu}$av Rider Jan. 74 (ENDF/B-IV)	$\bar{\nu}$av Rider May 73	$\bar{\nu}$av direct measurements
U235T	2.40	2.43	2.43
U235F	2.38	2.54	2.62
U235HE	3.80	4.27	4.48
U238F	2.75	2.93	2.80
U238HE	3.98	4.47	4.48
PU239T	2.92	2.89	2.87
PU239F	2.82	2.85	3.06
U233T	2.46	2.49	2.50

U233T – Rider Aug 73 – 2.48

[a]Using Terrell's summation method, Phys. Rev. <u>127</u>, 880 (1962)
calculated by K. Wolfsberg.

VII. CINDER-7 (T. R. England and N. Whittemore)

A completely reprogrammed version of the CINDER code is being debugged for limited operational use at LASL. This version uses a sophisticated data management system via the use of ~ 33 subroutines, many of which were converted from the obsolete ASCENT to COMPASS language.

The program is variably dimensioned, and essentially all parameters such as the number of time increments, nuclides per chain, time-dependent cross sections, etc., are variable depending on the total available storage. There are other new features such as calculation of delayed γ spectra and various new output options. The input data cards can be in any order, and data on the cards is not required to be in fixed fields.

Further changes in the type of input data, required storage and output summaries are being specified. The final changes will determine the input form required in the processing of ENDF/B-IV decay data.

VIII. NEUTRON FLUENCE TO DOSE CONVERSION (W. B. Wilson [Texas A&M], D. R. Harris, and D. G. Foster, Jr.)

The biological effect of radiation penetrating a shield is commonly measured in terms of the dose equivalent received by personnel at the shield boundary. Data for conversion of radiation fluence to dose equivalent thus are required for design of biological shields. Recent determinations of neutron fluence to dose equivalent, shown in Fig. 8, differ because of different selections of incident flux angular distributions, different phantom geometries, and different quality factors.[22-24] Also in Fig. 8 is a curve showing our selection of fluence to dose conversion values, $C(E_n)$, versus energy E_n, prepared as follows. The curve consists of linear segments on the log-log scale, so that interpolation is according to aE_n^b between tabulated pairs $(E_n, C(E_n))$. Below 5 keV, the curve passes through all the values of Rossi et al.[22] Above 5 keV, the curve passes through the values of Stevenson et al,[23] who use dose equivalent values averaged near the surface of the phantom rather than the peak dose equivalent values which may occur several centimeters inside the phantom. This technique is used so that fluence to dose conversion will satisfy requirements of cumulativity for incident neutron fluxes of different spectral composition.
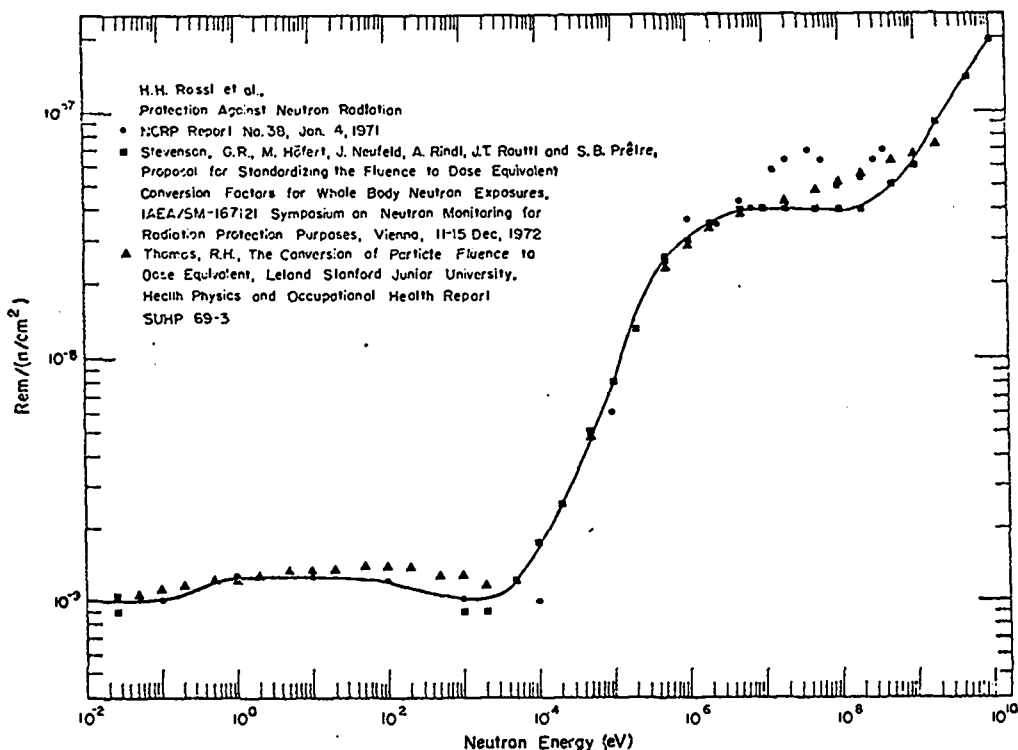

Fig. 8. Neutron fluence to dose equivalent conversion.

IX. NUCLEAR DATA FOR THE CONTROLLED FUSION PROGRAM (D. W. Muir, P. D. Soran, L. Stewart and P. G. Young)

One-hundred group neutron interaction cross sections have been prepared for vanadium and the results placed in the LASL/CTR processed nuclear data library. These cross sections were obtained by processing the ENDF/B-IV evaluation MAT 1196[25] using processing code MINX, recently developed at LASL. In the course of this work, the local interface code TINX was modified extensively to form a link between the MINX output tape and the LASL/CTR (DTF format) binary library tape. Also during this period, critical reviews of the ENDF/B evaluations for hydrogen, lithium, nitrogen, oxygen, and aluminum were prepared in response to a request from the CTR Subcommittee of the U. S. Nuclear Data Committee.

X. R-MATRIX ANALYSIS OF REACTIONS IN THE ^{7}Li SYSTEM (G. M. Hale, D. C. Dodder [T-9], P. G. Young, and L. Stewart)

The neutron-induced reactions on ^{6}Li are of interest in weapons design, and particularly important is the ^{6}Li(n,α)T cross section at low energies as a neutron "standard". We have focused the R-matrix analysis of reactions in the ^{7}Li system begun by Dodder on the problem of generating accurate n-^{6}Li cross sections in the vincinity of the 5/2- resonance at $E_n \approx 240$ keV. The analysis includes ^{4}He(t,t)^{4}He angular distributions and polarizations for triton lab energies below 11 MeV, ^{6}Li(n,n)^{6}Li angular distributions and polarizations for neutron lab energies below 2 MeV, and a few ^{6}Li(n,α) angular distributions below $E_n = 1$ MeV. Various sets of neutron total cross sections and integrated (n,α) cross sections have been analyzed with these data.

The total cross section measurements of Diment[26] appear to be most consistent with the other data in the analysis. However, the integrated (n,α) cross section predicted by the resulting resonance parameters is 15-20% higher than recent measurements by Coates,[27] Fort,[28] and Poenitz[29] near the 240-keV resonance. Attempts to force the calculated (n,α) cross sections to lower values have distorted the fits to other data in the analysis.

Very recent experimental developments may support the findings of the analysis. Preliminary measurements[30] of the n-^{6}Li total cross section at Oak Ridge National Laboratory appear to agree well

with the Diment data. New measurements by Friesenhahn[31] of the ^{6}Li(n,α) integrated cross section are 25% higher through the resonance than the data cited above. Finally, word comes from the recent EANDC meeting in Tokyo that corrections for the lithium content of the lithium-glass detectors will raise Fort's (n,α) cross sections by about 15%. The results of integral experiments indicate, on the other hand, that lower values of the (n,α) cross section are preferred.

It appears that precise values for these important cross sections are not yet known from experiments, and that an analysis such as ours that includes data from other reactions may be useful in determining them.

XI. R-MATRIX ANALYSIS OF REACTIONS IN THE ^{5}He SYSTEM (R. A. Nisley, G. M. Hale, and D. C. Dodder [T-9])

The reactions induced by deuterons on tritium are of great interest in the design of various fusion energy sources. We have therefore included the d-T channel in our R-matrix analysis of the n-^{4}He scattering, and extended the analysis above the d-T threshold. The reactions simultaneously under consideration are the T(d,n)^{4}He and T(d,d) reactions up to incident deuteron lab energies of 8 MeV and the ^{4}He(n,n) reaction up to incident neutron energies of 28 MeV. In addition to all the available cross section data, polarization data have been included where available. Of special note are the very recent measurements by G. Ohlsen (P-9) of outgoing neutron polarizations for polarized deuterons incident in the T(d,n) reaction at 7 MeV. These "polarization transfers" are the only measurements of this type in the energy region under study, and they may contribute significantly to the determination of the series of d-wave levels that occur near the upper end of the energy range. Even though three-body break-up has been neglected, the 2000 data points are fit with a chi-squared per degree of freedom of 5.7.

In addition, a simultaneous R-matrix analysis of the ^{5}He and ^{5}Li systems has been done through the d-T and d-^{3}He thresholds up to an incident deuteron energy of 1 MeV. This is an extension of earlier work where only the n-^{4}He and p-^{4}He elastic scattering were considered. A model to represent the

charge dependence of the R-Matrix parameters is still under investigation.

XII. R-MATRIX RESONANT ENERGIES (R. A. Nisley)

A short, user-oriented code has been developed to calculate resonant energies from multi-level, multi-channel R-matrix parameters. Relativistic kinematics are used to determine the arguments of the Coulomb functions.

A second code to transform the R-matrix parameters to an equivalent set under a change of boundary conditions has been developed.

XIII. CORRELATED ERROR FILES FOR ^{14}N and ^{16}O (P. G. Young, D. G. Foster, Jr., G. M. Hale, and D. M. McClellan)

One of the goals of the Defense Nuclear Agency's radiation transport program is to develop evaluated nuclear data sets and prediction techniques to the point that calculations of radiation transport can be performed to an accuracy of better than ± 25% in air and to better than ± 50% in materials other than air. In order to establish the accuracy of such calculations, however, estimates are needed of errors in the evaluated data, together with information about correlations in the data over both neutron energy and reaction type. For this purpose, estimates have been made of the covariance matrices of the neutron cross sections on the Los Alamos ^{14}N and ^{16}O evaluated data sets, and the results are available in the newly-adopted ENDF/B error format.

The errors are based upon estimates of the effect of covariances in the experimental data used for the evaluations and upon estimates of the correlations introduced by our analysis of the data. Only the important reaction types were considered, and no attempt was made to evaluate errors in the gamma ray production data or in secondary neutron angular distributions and energy spectra.

XIV. MISCELLANEOUS EVALUATION ACTIVITIES FOR VERSION IV OF ENDF/B (R. J. LaBauve, L. Stewart, and P. G. Young)

A number of miscellaneous activities have been carried out in preparing for the issuance of a new version (Version IV) of ENDF/B evaluated data. These activities include the following:

Phase I reviews were performed for the ^{12}C and ^{238}U evaluations that have been submitted for Ver-

sion IV. In the case of ^{238}U, direct inelastic scattering cross sections and second and third chance fission were added at high energies at the request of Paik from WARD.

The gamma-ray production files for ^{235}U and ^{239}Pu were modified according to the suggestions of Hutchins from General Electric. Other corrections and additions were made, including the File 1 comments for ^{235}U, and the complete ^{235}U file was compiled and sent to the Brookhaven National Laboratory Cross Section Center.

The gamma-ray production multiplicities and spectra for thermal neutron capture in the ^{182}W, ^{183}W, ^{184}W, and ^{186}W evaluations were revised to include a new measurement by Jurney of Los Alamos. The spectra were changed substantially for $E_\gamma < 1$ MeV.

Revisions were made to the ^{7}Li, ^{10}B, and ^{27}Al Version IV evaluations to correct minor problems revealed in Phase I reviews.

XV. MEDIUM ENERGY NUCLEAR DATA LIBRARY (D. G. Foster, Jr., D. R. Harris, and W. B. Wilson [Texas A&M])

A medium-energy nuclear data library is being appended to the ENDF/B library to permit more efficient medium-and low-energy particle and photon transport computations. Improvements continue in the intranuclear cascade/nuclear evaporation code that provides an immediate basis for the library; these computed data sets are being augmented by data evaluated from the experimental literature as time permits. Figure 9 shows dose equivalent computed from neutron fluxes at various points in a two-meter thick iron shield. These neutron fluxes were computed from DTF-IV using two 41-group neutron cross section decks, one computed from the intranuclear cascade/nuclear evaporation code and one modified to reflect measured reaction cross sections. The latter is about one fourth of the former outside the shield.

Both curves in Fig. 9 show transition effects near both the inner and outer shield walls. This behavior contrasts with that reported in Ref. 32.

It was thought advisable to repeat the iron penetration calculations, but for an iron shield only one meter thick so as to reduce statistical uncertainties in the NMTC Monte Carlo calculations. This problem also was employed to test the impor-
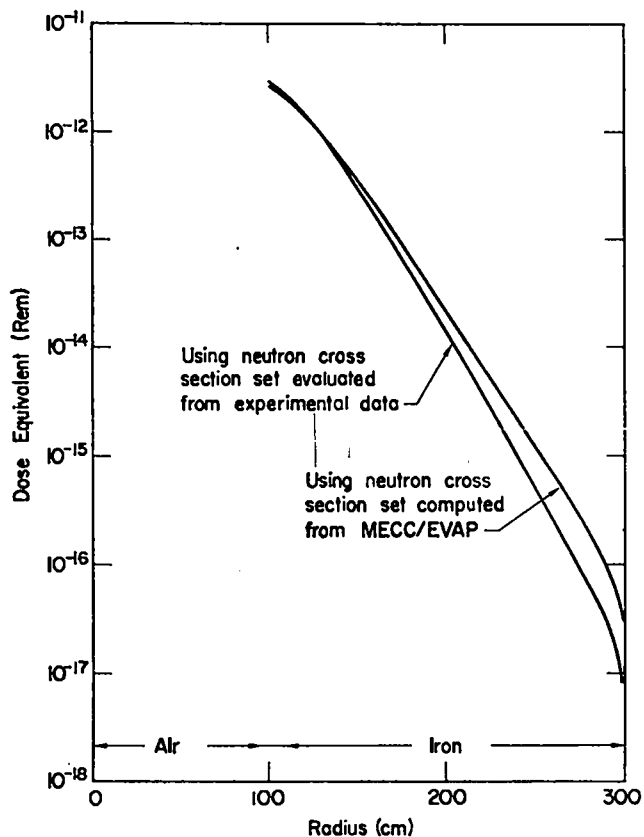
Fig. 9. Calculated dose equivalent for 2m
iron sphere test case.

for ancestors. Each of the four steps in the problem
was run to approximately 15,000 source particles.
The splitting-vs-energy feature of NMTC, which allows
the rare high-energy neutrons to be split in propor-
tion to their energy, was adjusted at each step to
maintain a yield of approximately 15,000 emerging
particles. After including the weights assigned dur-
ing the repeated splits, the 17,800 source neutrons
yielded 110 equivalent neutrons penetrating the meter
of Fe, of which 1.9 had charged intermediaries which
DTF could not have reproduced. Thus, the error due
to omission of charged-particle transport is less
than 2%. A second output tape was made from the
fourth run, containing histories of neutrons below
20 MeV deposited interior to the final 25-cm shell
of Fe. This tape can be used as a source for S_N cal-
culations also, in order to determine whether the
flux escaping the 200-cm surface would have been ap-
preciably enhanced by tracking the slow neutrons al-
so. Of the 838 neutrons in this distributed source,
3.5% have charged precursors. Thus, there is no in-
dication that the omission of charged-particle trans-
port causes an important error.

The dose equivalent above 20 MeV computed using
our medium-energy library neutron cross sections in
DTF is about 20% less outside the shield than the
dose equivalent computed from NMTC with compatible
cross sections. This difference is, of course, much
less than results from incorporating evaluated ex-
perimental cross sections as described earlier, but
it still is annoying. Use of various angular expan-
sions and transport corrections in the S_N calcula-
tions does not appreciably affect the results, as
was reported earlier. Figures 10 and 11 show dose
equivalent per unit neutron lethargy and neutron
fluence per unit neutron lethargy as computed from
S_N and Monte Carlo outside the shield. The shape of
the discrepancy is similar to that which would re-
sult from processing the neutron cross sections into
multigroup form assuming a neutron flux spectrum
varying as E^{-1} inside each group rather than a more
realistic spectrum. Thus the medium-energy multi-
group processor code DANA2 is being modified to in-
clude more realistic spectrum weighting.

tance of ignoring charged-particle transport and of
including various effects in the multigroup S_N trans-
port calculations.

Both NMTC and DTF use a common source spectrum
typical of LAMPF targets, in the center of a spheri-
cal void 100 cm in radius surrounded by an iron shell
100 cm thick. Since NMTC does not employ splitting at
internal boundaries, the NMTC case was run in four
25-cm steps. The neutrons above 20 MeV escaping
through a surface of radius 100 + 25n cm were re-
corded on tape and used as the source for a run in
which the iron shell extended between radii of 100
cm and 100 + 25(n+1) cm. The initial course was
filtered to use only the neutrons from the target.
In order to explore any limitation imposed by re-
stricting the transport to neutrons, NMTC was modi-
fied so as to tag all particles with the number of
precursors which were charged rather than neutral.
This contamination tag was propagated from step to
step, so that neutrons emerging from the 200-cm sur-
face which had a proton or pion ancestor could be
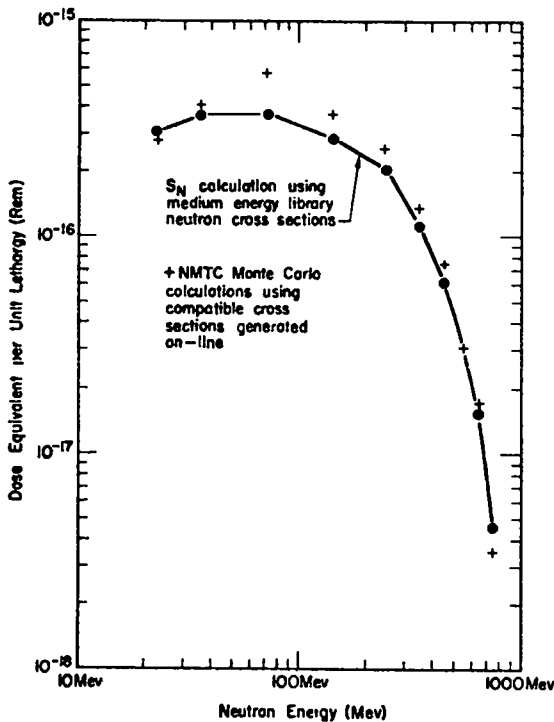distinguished from those which had only neutrons

Fig. 10. Dose equivalent per unit lethargy
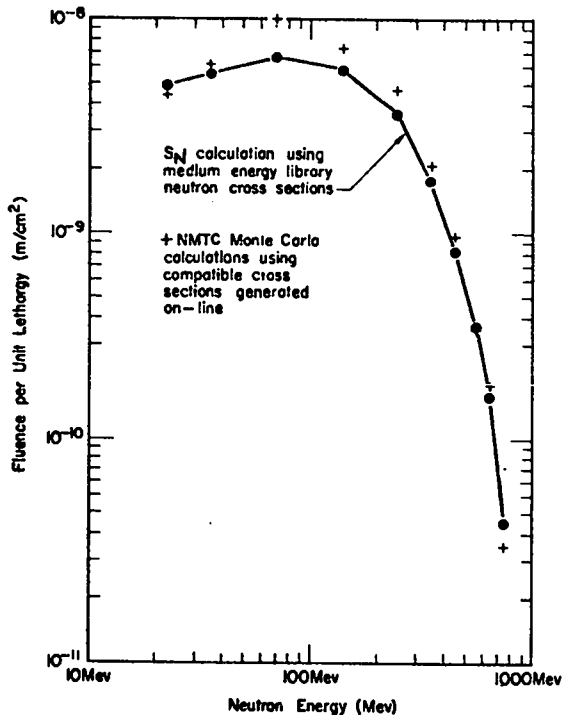for a 1m spherical test case.

Fig. 11. Fluence per unit lethargy for a 1m
spherical test case.

XVI. NASA EXTENSION OF MEDIUM ENERGY NUCLEAR DATA
LIBRARY TO 3.5 GeV   (D. G. Foster, Jr. and D.
R. Harris)

A program sponsored by NASA is underway to ex-
tend the medium-energy nuclear data library to 3.5
GeV for selected nuclei covering a wide range of
masses. Because the primary objective is dose cal-
culations in spacecraft and high-flying aircraft,
several light nuclei, notably C, O, and Al, are in-
cluded. For such light nuclei, there has been some
doubt as to the adequacy of the basic intranuclear-
cascade-plus-evaporation code CROIX at high incident-
particle energies, so before beginning systematic
calculations, a study has been undertaken of the
performance of CROIX for light nuclei.

CROIX was adapted from the Oak Ridge National
Laboratory code NMTC about four years ago and thus
is based on the MECC-3 intranuclear cascade module
together with the EVAP-3 evaporation module. The
parent code NMTC has evolved independently since
then at ORNL and at LASL. The ORNL version now uses
MECC-7 and EVAP-4, and differs mainly in the exten-
sive revision of the nucleon-nucleon and pion-pion
cross sections utilized by the code. In a companion
Oak Ridge code HETC, these cross sections have been
extended above the old limit of 3.5 GeV by a scaling
extrapolation which appears to be useful up to 1 TeV.
The LASL version has been revised mainly by the sub-
stitution of a more modern table of nuclear masses,
and by attempts to flag or eliminate some of the
more obvious errors. We plan to modify CROIX to
take advantage of some of these improvements before
carrying out the NASA calculations.

Some of the areas for which deficiencies have
been noted will be outlined here. These discrepan-
cies affect the residual nucleus energy and type and
can affect the production of low-energy neutrons.

Both MECC-3 and MECC-7 have an error in the
treatment of nucleon binding energy which permits
the intranuclear cascade to emit particles bearing
more than the incident energy, thus leaving the re-
sidual nucleus with a negative excitation energy.
The current LASL version of NMTC simply flags these
events and aborts the evaporation phase, which orig-
inally was allowed to proceed with a spurious posi-
tive excitation energy to drive it. In a test calcu-
lation for 800-MeV neutrons on ^{16}O about 45% of the
cascades exhibited this error, with an average over-

shoot of 5.1 MeV and a maximum of 16.8 MeV. This problem arises partly from conceptual difficulties in defining the binding energy in the course of the intranuclear cascade and partly from practical difficulties in determining the actual sequence of escape from the nuclear surface. Since the alternatives are to ignore this problem or to discard the unphysical events after completing the cascade calculation (which would increase the cost of computation and which might be biased), the feasibility of such a correction is being explored.

The EVAP module has at least three problems which are aggravated in light targets: 1. Creation of impossible residual nuclei such as those with negative neutron number; 2. Errors in overall energy balance when the residual nucleus is in the range of particle types which EVAP emits during evaporation; and 3. Occasional failure to emit a particle when emission is energetically possible. In collaboration with P. Seeger, several of these errors have been located and corrected. The first occurs mainly for residual nuclei which lie outside the boundaries of the mass table, and can be corrected by suitable extrapolation for nuclei very far on the neutron-poor side of the line of stability. The second problem produces errors as large as 50 MeV, and is the result of at least two straightforward programming errors. When the residual nucleus is itself an "emittable" particle, it is not being given the recoil energy when it is transferred to the table of emitted particles. In addition, in certain cases when an energetically possible emission fails to occur, the emission has already been tabulated and is not erased. The latter is a by-product of the third problem, which involves an inefficiency in sampling the temperature model of the density of states in the residual nucleus for emission close to threshold. All of these appear to be readily correctable.

XVII. NUCLEAR DATA FOR DESIGN OF A ^{9}Be(d,xn) NEUTRON RADIOTHERAPY SHIELD (W. B. Wilson [Texas A&M] and D. R. Harris)

The University of Texas M. D. Anderson Hospital and Tumor Institute and Texas A&M University are conducting clinical trials of fast neutron cancer therapy. These trials are being carried out at the Cyclotron Institute of Texas A&M with the support of the National Cancer Institute (Grant CA-12542-01).

Using a beam of 50-MeV deuterons produced by the cyclotron, an intense, anisotropic, forward-peaked source of fast neutrons is produced by the reaction ^{9}Be(d,xn). This fast neutron source must be collimated to produce the desired effect, while neutrons not directed at the tumor must be shielded from healthy tissue.

The required collimator-shield is being designed using the one- and two-dimensional discrete ordinates code DTF-IV[33] and TWOTRAN[34] together with modifications of the LASL multigroup medium- and low-energy neutron cross-section library.[35] Alternative cross section and transport treatments, and alternative gross material rearrangements, are being studied in spherical geometry with the neutron source spectrum taken to be that in the forward direction from the ^{9}Be(d,xn) reaction.

Figure 12 shows neutron dose equivalents associated with neutron flux distributions through 66-cm shields of iron, lead, and tungsten calculated using a standard 34 group neutron cross-section set. The neutron flux-to-dose conversions used in this calculation are described elsewhere in this report. Tungsten appears to be a superior shield material from the neutron transport point of view, but because of its cost, combinations of iron with tungsten near the source also are being considered.
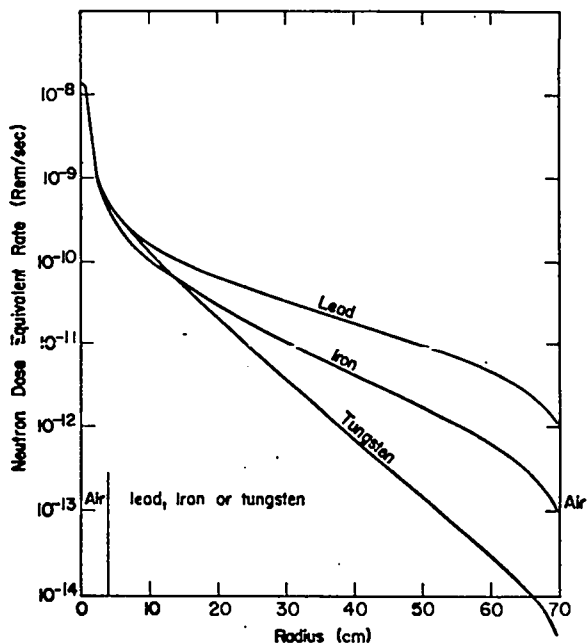

Fig. 12. Neutron dose equivalent rate through 66-cm lead, iron, and tungsten shields for Unit ^{9}Be(d,xn) neutron source.

A series of calculations for a spherical iron shield have shown that results are relatively insensitive to order of Legendre expansion (P_3-P_8) of the multigroup cross sections, to use of a diagonal transport correction, to number of spatial mesh points (74-140) in the iron, to angular quadrature sets (S_8-$S16$), and to alternative convergence criteria. Even the use of evaluated cross sections 15% to 25% higher in the 17-60 MeV range decreased the transmitted dose equivalent by only 10%, partly because only about 60% of the source neutrons are emitted in this energy range and partly because there is a transition effect for shields of about this thickness. That is, the higher cross sections are associated with a larger dose equivalent at the inner face of the shield, a smaller dose equivalent at the outer face of the shield, and a crossover about 20 cm deep in the shield.

XVIII. HTGR XENON-POWER STABILITY (T. R. England and D. R. Harris)

A preliminary examination of the HTGR spatial stability to xenon-power oscillations was made. The analysis used an improved criterion but required some neutronics parameters derived from data in the Fulton Plant's PSAR. The conclusions therefore are essentially a check on the reported criterion for stability used in the PSAR.

In general, it appears that the core will be stable if the overtone eigenvalues are ~ 2.4% larger than the fundamental mode eigenvalue. The reported eigenvalue difference is 3% axially and 1.9% radially. Accordingly, a negative power coefficient is necessary to achieve the design requirement of stability. The reported moderator coefficient is positive but reported Doppler coefficient is sufficiently negative to achieve a net negative coefficient to force radial stability. The Doppler coefficient results primarily from the ^{232}Th loading, although the ^{235}U coefficient is, surprisingly, a large negative value.

The ^{232}Th loading is essential to radial and axial stability. The reported eigenvalue differences appear to be very large for a reactor as large as the Fulton Plant (~28' in diameter and 21' high). The relatively small Shippingport reactor (6'x6') had a radial plane eigenvalue difference of only ~ 1.5% and was unstable. Accordingly, independent

calculations of the eigenvalue separations, relativity coefficients, and thermal spectrum averaged xenon cross sections are needed for any final conclusion on stability. The means used in determining these parameters is not described in the Fulton PSAR, nor is there any indication that parameter variations during reactor lifetime and some spatial effects were considered. Potential control problems were not considered in this preliminary analysis.

Questions on the details used by GA in their examination of stability will be explored in a meeting scheduled for late April.

REFERENCES

1. D. R. Harris, R. J. LaBauve, R. E. MacFarlane, P. D. Soran, C. R. Weisbin, and J. E. White, "MINX, A Modular Code System for Processing Multigroup Cross Sections from Nuclear Data in ENDF/B Format," Los Alamos Scientific Laboratory report LA-UR-1766, Jan. 1973.

2. Private Communication.

3. M. Raymund, "TEDIUM: Idealized Neutron Data for Testing Library Processing Codes," ANS Reactor Physics Division Topical Meeting on New Methods in Reactor Physics, CONF-720901, p. 1048 (1972).

4. M. Raymund, private communication (1974).

5. J. C. Vigil, "Service Modules for Version II Standard Interface Data Files," Los Alamos Scientific Laboratory report LA-5367-MS (August 1973).

6. C. R. Weisbin and R. J. LaBauve, "Specifications of a Generally Useful Multigroup Structure for Neutron Transport," Los Alamos Scientific Laboratory report LA-5277-MS (1973).

7. R. E. Schenter, J. L. Baker, and R. B. Kidman, "ETOX, A Code to Calculate Group Constants for Nuclear Reactor Calculations," Battelle Northwest Laboratory report BNWL-1002 (1962).

8. R. J. LaBauve, R. E. Seamon, C. R. Weisbin, D. R. Harris, and D. W. Muir, "Development of ENDF/B Shielding Data, Processing Codes, and Integral Tests," ANS Reactor Physics Division Topical Meeting on New Methods in Reactor Physics, CONF-720901, pp. 316-324 (1972).

9. A. Travelli, "FFTF Critical Assembly Experiments Planning and Evaluation," Argonne National Laboratory report ANL-7669, pp. 17-25 (1970).

10. D. W. Muir, R. J. LaBauve, and R. E. Alcouffe, "Analysis of ZPPR/FTR-2 Neutron Reactions Rates Using ENDF/B-III Data," Trans. Am. Nucl. Soc. 16, 337 (1973).

11. E. T. Boulette and W. L. Bunch, "Analysis of ZPPR/FTR Shield Experiments: Gamma Distribution," Westinghouse Electric Corporation report WHAN-FR-13 (1971); also E. T. Boulette, W. L. Bunch, and L. F. Kocher, "ZPPR/FTR-2 Shield Experiments: Gamma Distribution," Trans. Am. Nucl. Soc. 13, 400 (1970).

12. D. J. Dudziak, R. E. Seamon, and D. V. Susco, "LAPHANO: A P_0 Multigroup Photon-Production Matrix and Source Code for ENDF," Los Alamos Scientific Laboratory report LA-4750-MS (ENDF-156) (1972).

13. B. J. Toppel, A. L. Rago, and D. M. O'Shea, "MC^2, A Code to Calculate Multigroup Cross Sections," Argonne National Laboratory report ANL-7318 (1967).

14. E. F. Plechaty and J. R. Terrell, "Photon Cross Sections 1 keV to 100 MeV," University of California/Livermore report UCRL-50400, Vol. VI (1968).

15. K. D. Lathrop, "GAMLEG – A FORTRAN code to Produce Multigroup Cross Sections for Photon Transport Calculations," Los Alamos Scientific Laboratory report LA-3267 (1965).

16. K. D. Lathrop and F. W. Brinkley, "Theory and Use of the General Geometry TWOTRAN Program," Los Alamos Scientific Laboratory report LA-4432 (1970).

17. Argonne National Laboratory Staff, "Reactor Physics Constants," Argonne National Laboratory report ANL-5800, pp. 7.4.1 (1958).

18. G. G. Simons and T. J. Yule, "Gamma-Ray Heating Measurements in Zero-Power Fast Reactors with Thermoluminescent Dosimeters," Nucl. Sci. Eng. 53, 162 (1974).

19. C. L. Wingate, E. Tochilin, and W. Goldstein, "Response of Lithium Fluoride to Neutrons and Charged Particles," Proc. Conf. Luminescence Dosimetry (Stanford), June 21-23, 1965.

20. D. R. Harris and J. M. Wallace, "Calculations of Multigroup Cross Sections and Transfer Matrices for Target Nuclei with Arbitrary Velocity Distributions," Trans. Am. Nucl. Soc. 17, 548 (1973).

21. K. D. Lathrop, "DTF-IV, A FORTRAN-IV Program for Solving the Multigroup Transport Equation with Anisotropic Scattering," Los Alamos Scientific Laboratory report LA-3373 (1965).

22. H. H. Rossi et al, "Protection Against Neutron Radiation," National Council of Radiation Protection report No. 38 (January 1971).

23. G. R. Stevenson, M. Hofert, J. Neufeld, A. Rindi, J. T. Routti, and S. B. Pretre, "Proposal for Standardizing the Fluence to Dose Equivalent Conversion Factors for Whole Body Neutron Exposures," IAEA/SM-167/21 Symposium on Neutron Monitoring for Radiation Protection Purposes, Vienna (December 1972).

24. R. H. Thomas, "The Conversion of Particle Fluence to Dose Equivalent," Leland Stanford Jr. University, Health Physics and Occupational Health Report SUHP-69-3.

25. S. K. Penney and L. W. Owen, "A Reevaluation of Vanadium Neutron and Gamma-Ray Production Cross Sections," Oak Ridge National Laboratory report ORNL-TM-4007 (1972).

26. K. N. Diment and C. A. Uttley, "The Total Cross Section of ^{6}Li," Atomic Energy Research Establishment report AERE-PR/NP15; also private communication from C. A. Uttley to L. Stewart.

27. M. S. Coates, G. J. Hunt, and C. A. Uttley, private communication to L. Stewart (1973).

28. E. Fort and J. P. Marquette, private communication to L. Stewart from M. Coates (1973).

29. W. P. Poenitz, private communication to L. Stewart (1973).

30. J. A. Harvey and N. W. Hill, private communication (1974).

31. S. J. Friesenhahn, private communication (1974).

32. R. G. Fluharty, P. A. Seeger, D. R. Harris, J. J. Koelling, and O. L. Deutsch, "Transport of Neutrons Induced by 800-MeV Protons," Los Alamos Scientific Laboratory report LA-UR-73-200, presented at Symposium on Applications of Nuclear Data in Science and Technology, Paris, France, March 12-16, 1973.

33. K. D. Lathrop, "DTF-IV, A FORTRAN-IV Program for Solving the Multigroup Transport Equation with Anisotropic Scattering, Los Alamos Scientific Laboratory report LA-3373 (1965).

34. K. D. Lathrop, "Users Guide for the TWOTRAN Program," Los Alamos Scientific Laboratory report LA-4058 (1969).

35. D. R. Harris et al, "Medium- and Low-Energy Neutron Cross Section Library," Trans. Am. Nucl. Soc. 15, 962 (1972).

PUBLICATIONS

1. P. G. Young, "Cross Section Evaluation for N, O, Al, Ag, Sn, and W," Invited paper for Radiation Physics Division Radiation Transport Information Meeting, Washington, D. C., March 1974.

2. D. C. Dodder, G. M. Hale, R. A. Nisley, K. Witte, and P. G. Young, "Models Based on Multichannel R-Matrix Theory for Evaluating Light Element Reactions," Los Alamos Scientific Laboratory report LA-UR-74-738, presented by H. T. Motz at EANDC Topical Discussion on Critiques of Nuclear Models and Their Validity in the Evaluation of Nuclear Data, Tokyo, March 1974.